Considerations on Iron Nitride Enabled Rare Earth Free Hybrid Variable Flux Machines

Julius Kesten
Institute of Electrical Engineering
Karlsruhe Institute of Technology
Karlsruhe
julius.kesten@kit.edu

Matthias Brodatzki
Institute of Electrical Engineering
Karlsruhe Institute of Technology
Karlsruhe
brodatzki@kit.edu

Martin Doppelbauer
Institute of Electrical Engineering
Karlsruhe Institute of Technology
Karlsruhe
martin.doppelbauer@kit.edu

***Abstract*—A potential analysis for the application of iron nitride magnets in (hybrid) variable flux machines ((H)VFM) is presented, investigating the possibility to design rare earth free machines using ferrite and iron nitride magnets. A review on variable flux machine research is given to contextualize the presented work. Delta topology machines with different magnet combinations are simulated using design of experiments. The magnetization characteristics of the machines are investigated by directly deriving the magnetic fields in the machines' permanent magnets from the vector potential in the single mesh elements. Series HVFM machines using magnet alloys with strongly different remnant magnetization are discussed. The performance of different (H)VFM is compared with regard to their ability to demagnetize, the demagnetization characteristics in the torque-speed plane and the overall performance. Series HVFM with iron nitride and ferrite magnets are challenging due to demagnetization of the iron nitride magnets.**

***Index Terms*—variable flux machine, iron nitride, demagnetization, series hybrid variable flux machine**

I. Introduction

With market shares of electrified transportation growing, sustainable solutions to provide the increasing demand for electric traction systems need to be investigated. Most modern traction systems rely on rare earth enabled permanent magnet synchronous machines (PMSM) to generate propulsion. However, rare earth materials are expensive, are only recycled in small amounts and pose a risk in supply chains [1].

To mitigate these risks, alternate machine topologies are investigated, such as (hybrid) variable flux machines ((H)VFM). The conventional variable flux machines employ so-called semi hard magnets, such as AlNiCo or ferrite alloys. Owing to their low coercive forces, these magnets can be de- and re-magnetized during machine operation by applying adequate stator current (d-current) pulses. A schematic representation of this process is shown in Fig. 1. Once the magnitude of the applied current in the d-axis is sufficiently large, the d-axis flux linkage Ψ_d is reduced even after the current returns to 0, with $\Psi_\mathrm{d}|_{i=0} = \Psi_\mathrm{PM}$. This is due to the demagnetization of the rotor magnets. The process can be reverted by applying a sufficiently large, positive d-current. (H)VFM operate with regular multiphase stators and require no additional parts in the rotor [2], [3]. A magnetization state (MS) is introduced, representing the permanent magnet (PM) flux linkage $\Psi_\mathrm{PM,mom}$ related to the maximum PM flux linkage $\Psi_\mathrm{PM,max}$ at full magnetization as

$$MS = \frac{\Psi_\mathrm{PM,mom}}{\Psi_\mathrm{PM,max}}. \tag{1}$$

In hybrid VFM, there are both a set of high coercive force (HCF) and low coercive force (LCF) magnets, either arranged in series or parallel. The placement of the respective magnets in the rotor is schematically represented in Fig. 2. While the advantage of parallel structures is a greater range of adjustable magnetization with a lower output torque, series topologies

This work was in part financed through the Ministry of Science, Research, and Arts of the Federal State of Baden-Württemberg, Germany, in the framework of "Innovationscampus Mobilität der Zukunft"

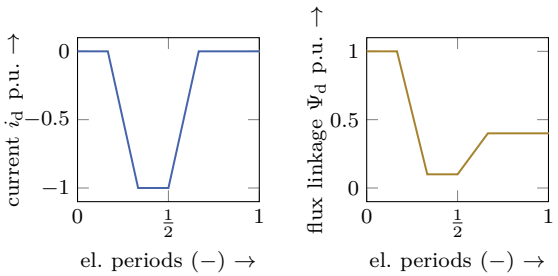

(a) d-current ramp (b) d-flux linkage

Fig. 1: Demagnetization process, schematic representation with the d-axis current ramp applied (a) and the resulting behavior of the d-axis flux linkage (b).

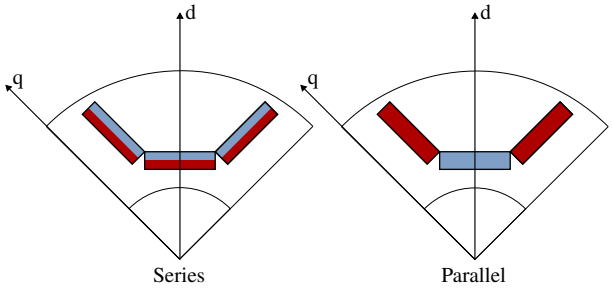

Fig. 2: Series (left) and parallel (right) topologies in HVFM with radial magnetization, HCF magnets in red, LCF in blue.

© 2026 IEEE. Personal use of this material is permitted. Permission from IEEE must be obtained for all other uses, in any current or future media, including reprinting/ republishing this material for advertising or promotional purposes, creating new collective works, for resale or redistribution to servers or lists, or reuse of any copyrighted component of this work in other works.

have more stable working points of the LCF magnets and further enable easier re-magnetization, while having larger output torque [4]. However, this comes at the cost of a reduced range of applicable MS. The HCF magnets are typically comprised of NdFeB alloys, while the LCF magnets are AlNiCo or ferrite ones, as in regular VFM [5]–[7]. To make use of both topologies, combinations of parallel and series machines were proposed [8], [9].

Recently, the novel permanent magnetic alloys based on iron nitride (FeN) were introduced for utilization in electric machines and investigations into their application for electric machines were carried out for conventional PMSM and VFM [10], [11]. This material presents with large remanence and coercive forces, the latter comparable to those of high-performance ferrite magnets [11]–[13]. One of the main problems of FeN appears to be mechanical stability: The magnetic properties cited are achieved in nano films rather than magnet blocks [14]. The BH data regarding FeN magnets presented in this work in Fig. 3 is based on the hysteresis curve presented in [11].

The performance of (H)VFM is in part determined and limited by the LCF magnets. The maximum operating current under full magnetization is determined by motor topology, as the combination of stator current and machine geometry is directly responsible for the external fields acting on the magnets. It is therefore useful to define an expected operating current in the design process and make the magnets' working point part of the optimization process [15].

While the LCF magnets should have a constant working point during normal operation, the ability to change their magnetization is important for inverter design as it determines the maximum required currents. These magnetization characteristics can be represented in current dependent magnetization maps as presented in [10], where the required d-q-current combination to magnetize or demagnetize the magnets to a certain working point is represented.

The aim of this work is to investigate the novel FeN magnets and their applicability in HVFM. The FeN magnets are used as LCF magnets. High performance ferrite magnets are used as HCF magnets. Machines with AlNiCo LNGT80 magnets are used for comparison. The behavior of the magnets regarding undesired demagnetization during normal operation is described. The focus thereby lies on the series HVFM. The effects of the starkly different remanence flux densities and the effects on the machines' performance is discussed.

The paper is structured as follows: in section II the approach to identifying the magnets' load and the machines investigated in this work are presented. Section III gives an overview over the simulations that were carried out and the results of these are presented and discussed in section IV. A summary and an outlook are given in section V.

II. Model

The BH data of all magnets used in this work is represented in Fig. 3. The ferrite magnet's critical field lies in the third

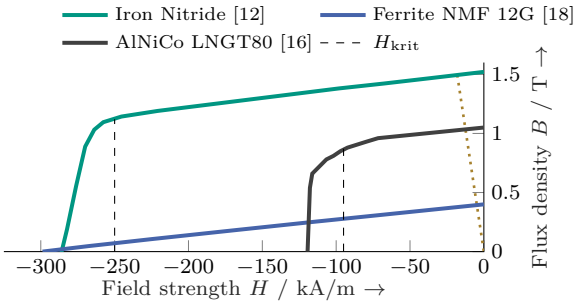

Fig. 3: BH curves of the magnets and rotor topologies investigated [11], [16], [18].

quadrant of the BH plane, making accidental demagnetization during operation unlikely.

For the BH curves of the AlNiCo and FeN magnets, the critical field strength H_{crit} is included as a dashed line in Fig. 3. It represents the magnitude of external fields loading the magnet, from which on demagnetization occurs. In this case, the magnet will not return to its original operating point (OP) on the curves in Fig. 3 but rather to a new OP with reduced flux density, following along a recoil line parallel to the linear area of the magnet's BH curve. The operating point settles then again on the load line, presented dotted orange in the figure [16], [17].

A. Volume based demagnetization calculation

To enable the analysis of machine designs created with design of experiment (DoE), i.e. large quantities of machines simulated through FEA, adequate strategies are required. To investigate the utility of FeN magnets in HVFM, the external magnetic fields acting on the rotor magnet, i.e. the magnets' OP, are analyzed. The FEA mesh in the magnets is used to calculate the quantities of interest, such as the flux density $\vec{B}$ and the magnetic field strength $\vec{H}$, directly from the magnetic vector potential $\vec{A}$ based on the methodology presented in [19]: The relation between $\vec{A}$ and $\vec{B}$

$$\vec{B} = \nabla \times \vec{A} \tag{2}$$

with the nabla operator ∇ is used. Since the FEA is solved in a 2D plane the relation between flux density and vector potential simplifies to

$$\nabla \times \vec{A} = \begin{cases} \frac{\partial A_{\mathrm{z}}}{\partial y} - \frac{\partial A_{\mathrm{y}}}{\partial z} & = B_{\mathrm{x}} \\ \frac{\partial A_{\mathrm{x}}}{\partial z} - \frac{\partial A_{\mathrm{z}}}{\partial x} & = B_{\mathrm{y}} \\ \frac{\partial A_{\mathrm{y}}}{\partial x} - \frac{\partial A_{\mathrm{x}}}{\partial y} & = 0. \end{cases} \tag{3}$$

With the knowledge of the rotor position and the magnetization direction of the magnets it is possible to calculate the flux density components in normal B_{n} and tangential B_{t} direction relative to the magnets for each mesh element of interest [19].

With this information the hystersis curve of each magnet is used to determine its OP. Owing to the geometry's discretization into polygonal mesh elements, an individual element's proportion of a magnet's cross section can be

derived. Since (3) is evaluated for each mesh element in each magnet, the volume based demagnetization of each individual magnet can be determined by comparing the magnet's OP to its intrinsic H_{crit}, as shown in Fig. 3. In the work presented here, the investigated criterion is purely whether a mesh element is subjected to a field with a magnitude larger than that of the critical field, and the demagnetization by volume is calculated based upon this information. It is, however, possible to derive further information, such as the relative demagnetization compared to a magnet's B_{rem}.

The FEA results are current dependent maps for quantities such as the flux linkages $\Psi_{\mathrm{U}}, \Psi_{\mathrm{V}}, \Psi_{\mathrm{W}}$ in each phase, the iron losses $P_{\mathrm{fe,R}}, P_{\mathrm{fe,S}}$, in rotor and stator respectively, or the induced voltages. These maps are recorded for a given speed. Based on them, the characteristic speed torque envelopes and efficiency maps of the simulated machines are calculated in post processing. In this step, the demagnetization data, which is also saved in current dependent maps, is calculated for the torque speed plane of the machine as well. Thus, the demagnetization by volume percentage for each magnet is available for the machine's entire operating range.

B. Series magnet interface investigation

To determine the effect of the series configuration, the interface condition

$$\left(\vec{B}_1 - \vec{B}_2\right) \cdot \vec{n}_{12} = 0 \tag{4}$$

is considered, where the magnetic behavior of different materials on an interface is described, with the flux density vectors to either side of the interface $\vec{B}_1$ and $\vec{B}_2$ and the normal vector on the interface $\vec{n}_{12}$. Eq. (4) effectively states, that the normal part of the flux density to either side of an interface must be equal. For a series HVFM the assumption can be made that $\vec{B} = B_{\mathrm{n}}$ is valid on the interface between both magnets, with the normal component of the flux density B_{n}. As long as the flux density is homgoenous along the direction of magnetization, it follows: $B_{\mathrm{HCF}} = B_{\mathrm{LCF}}$. Effectively, both magnets must therefore find an equilibrium where (4) is satisfied.

This relation is presented in Fig. 4: The flux density in the operating point in this example is $B_{\mathrm{OP}} \approx 0.6\,\mathrm{T}$. Due to the nonlinear behavior of the LCF magnet's BH curve, the relative permeabilities $\mu_{\mathrm{r,i}}$ and therefore the resulting fields H_{ext} differ. If the difference in between the HCF magnet's remanence $B_{\mathrm{rem,HCF}}$ and the LCF magnet's remanence $B_{\mathrm{rem,LCF}}$ is too large or the LCF coercity $H_{\mathrm{c,LCF}}$ is too low, demagnetization of the LCF magnet will occur already under no-load conditions.

C. Machine model

A delta base topology is investigated in this work, as presented in Fig. 5. The magnets are split perpendicularly to their direction of magnetization. DoE enabled FEA simulations are carried out varying the rotor geometry only. Latin hypercube sampling (LHS) is employed as statistical sampling method to generate the variations for the DoE. There are

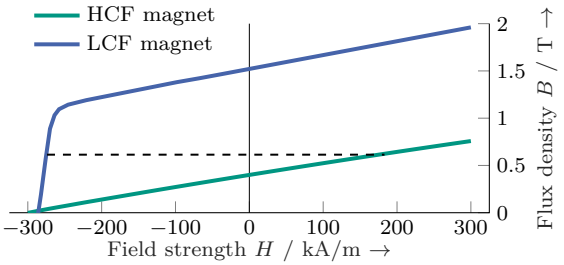

Fig. 4: BH-working points of LCF and HCF in a series configuration.

TABLE I: Common properties of the simulated machines.

Property	Value	Unit
Outer diameter D_{o}	120	mm
Bore diameter D_{b}	80	mm
Air gap length δ	0.5	mm
Length l_{fe}	80	mm
No. of slots N_{s}	36	-
No. of pole pairs p	3	-
No. of conductors per coil Z_{c}	10	-
Parallel branches a	1	-
Rated current I_{rms}	45	A
DC link voltage U_{dc}	400	V
Max. speed n_{max}	15000	1/min

three sets of simulations carried out. A set of machines using AlNiCo magnets only is used as a base line to compare the other machines to. Further, machines using FeN magnets only are analyzed. Lastly a dataset with FeN-ferrite hybrid machines is investigated.

The same three-phase stator is used for all machines with the geometrical and electric properties given in Table I.

A parametrized geometry is used, where the partition of the magnets is added. The geometry's main features are presented in Fig. 5. The width (M_{W}) and thickness (M_{T}) of the magnets are adjusted in the DoE, as well as their radial position inside the rotor (H). In the case of magnet 2, the value H_2 defines the length of the v-shape while keeping the opening angle α_2 constant. Effectively it determines the burial depth of the iron web at the bottom of the v-shape. Both flanks of the v-shape are equal, which is why only one of the magnets in this position is parametrized. The angle α_2 determines the opening angle of the v-shape.

An additional parameter M_{R} determines the ratio between the LCF and HCF magnets' thickness, thereby enabling the analysis of HVFM. It is defined as

$$M_{\mathrm{R}} = \frac{M_{\mathrm{T,HCF}}}{M_{\mathrm{T,total}}} \tag{5}$$

with the thickness of the HCF magnet $M_{\mathrm{T,HCF}}$ with regard to the total thickness $M_{\mathrm{T,total}}$ of the respective magnet. The ratio divides the magnet accordingly within the respective thickness $M_{\mathrm{T},i}$ presented in Fig. 5. The full list of DoE parameters including their variation range is presented in the bottom part of Table II. The parameter $M_{\mathrm{R},i}$ denotes the magnet ratio as given in (5).

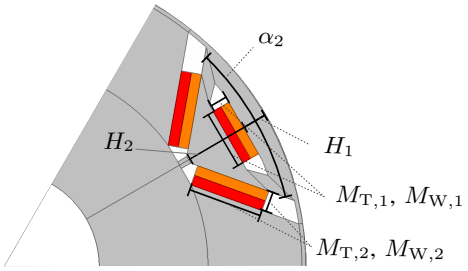

Fig. 5: Rotor topology investigated in this work, red HCF magnets, orange LCF.

III. Simulation

All FEA calculations presented in this work are carried out in Ansys Electronics.

The FeN magnet material was modeled in Ansys as a non-linear permanent magnet using the hysteresis curve presented in Fig. 3. No thermal modification was added.

The different machine configurations are simulated taking the number of variation parameters into account: for the hybrid version there are two additional parameters, which is why the size of the DoE was increased from 500 machine variations for the normal machines to 750 variation for the hybrid ones. Invalid parameter combinations may occur, resulting in a discrepancy between the initial size of the DoE and the actual number of successfully simulated machines. The corresponding data is given in the top part of Table II, where the success rate represents the percentage of successfully completed FEA simulations in relation to the size of the DoE. The success rate beyond $95\,\%$ for all magnet combinations suggests a sensible selection of the variation parameters' range.

TABLE II: Simulated machine combinations, top: DoE data, bottom: range of variation parameters.

Magnet material	**Size of DOE**	**Success rate / %**
AlNiCo	500	95.60
FeN	500	96.00
Hybrid	750	97.07
Variation parameter	**Range**	**Unit**
$M_{\mathrm{T},1,2}$	$1.5-3$	mm
$M_{\mathrm{W},1,2}$	$5-12$	mm
H_1	$1-5$	mm
H_2	$11-17$	mm
α_2	$90-110$	°
$M_{\mathrm{R},1,2}$	$0.2-0.8$	–

IV. Results

The torque-speed envelopes of the simulated machines with the different magnet combinations are presented in Fig. 6, where the y-axis on the left presents the mechanical shaft torque T_{sh} and the right y-axis the mechanical output power P_{sh}. The AlNiCo machines have the the lowest performance in the comparison, which is to be expected

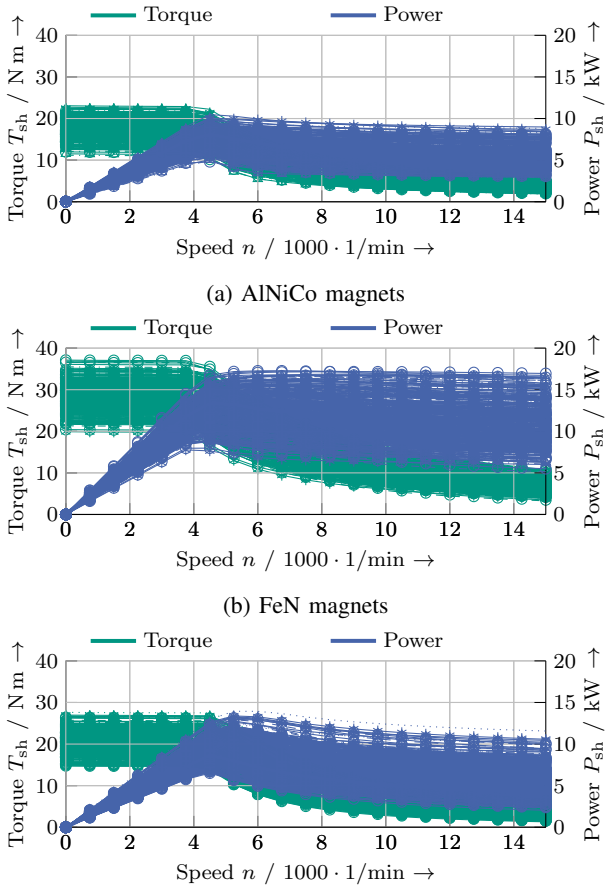

(a) AlNiCo magnets

(b) FeN magnets

(c) Hybrid magnets

Fig. 6: Torque-speed envelopes of the simulated machines for all magnet material combinations used.

considering their magnetic properties as presented in Fig. 3. The FeN machines exceed the hybrid machines' maximum torque and consequently power. The range in which the performance varies for either machine type is similar. The FeN machines consistently present with nearly constant power in the field weakening range. Contrary to what is expected of series HVFM according to the considerations discussed in section I and [4], the FeN machines exceed the hybrid ones performance-wise. This is due to the difference in remanence flux density B_{rem} between both machines, as described in section II-B.

This relation is represented in Fig. 7 for a generic delta machine, where the external fields $\vec{H}$ acting on either magnet are given as an extract from the FEA simulation for an exemplary machine. There is no load acting on the magnets other than the magnetic resistance of the machine's air gap and iron circuit i.e. $i = 0$. While the FeN magnets, presented in orange, are loaded by a negative field, the ferrite magnets are subject to a positive field. Typically a permanent magnet in a magnetically resistive circuit, as is an electric machine with the air gap and iron resistances, would be subjected to a negative magnetic field (external field). This indicates that the

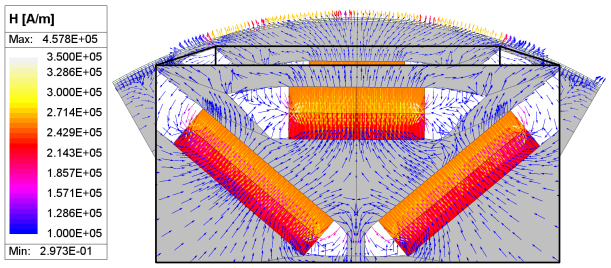

Fig. 7: Detailed view of fields acting on the magnets in the hybrid delta machine under no-load conditions.

FeN magnets with the larger B_{rem} are effectively magnetizing the ferrites and in the process become demagnetized beyond the critical knee point, with external fields reaching up to $H_{\mathrm{load}} \approx 275\,\mathrm{kA/m}$ in magnitude in the given example.

These FEA results confirm the assumptions with regard to (4) presented in section II-B.

This pre-load acting on the LCF magnets negatively impacts the hybrid machines' performance. The overall effect can be recognized when considering the machines' LCF magnets' volume based demagnetization throughout their operating range. This investigation is exemplarily carried out on two delta machines: One is a non-hybrid FeN machine, the other one is an FeN-ferrite hybrid one. For both machines, magnet 2 (see Fig. 5) is investigated. Both machines are selected for their maximum shaft torque $T_{\mathrm{max}} = T_{\mathrm{sh,max}} \approx 25\,\mathrm{N\,m}$ out of the DoE datasets.

In Fig. 8 the demagnetization by volume percentage for the selected FeN (Fig. 8a) and the hybrid (Fig. 8b) machine is compared. The data presented in Fig. 8 refers to the FeN magnet in either machine, i.e. the ferrite magnet is not represented in Fig. 8b. While the FeN machine has full magnetization up to approx. $17\,\mathrm{N\,m} \approx 0.68 \cdot T_{\mathrm{max}}$, the magnet in the hybrid machine is fully demagnetized at approx. $8\,\mathrm{N\,m} \approx 0.32 \cdot T_{\mathrm{max}}$. Also, the hybrid machine requires $60\,\%$ more magnet material by volume in total to generate the same output torque.

A VFM's capability of MS changes can be investigated with demagnetization maps, as presented in [10]. Here, a demagnetizing current pulse I_{demag} of a certain magnitude and current angle ϑ (i.e. the angle between the q-axis and the current phasor in the d-q-plane) is applied to the machine and the residual flux linkage after reducing the current back to $0\,\mathrm{A}$ is analyzed (see Fig. 1). The resulting demagnetization maps for both selected machines are visualized in Fig. 9 for current magnitudes of up to $I_{\mathrm{demag}} = 3 \cdot I_{\mathrm{nom}}$. Fig. 9b shows that albeit the FeN magnets in the hybrid machine demagnetize beyond their H_{crit} (see Fig. 8b), it is not possible to demagnetize the rotor completely due to the ferrite magnets' large coercivity: The minimum magnetization state achieved with the hybrid machine is $MS_{\mathrm{hyb,min}} \approx 30\,\%$ as compared to $MS_{\mathrm{FeN,min}} \approx 0\,\%$ in the FeN machine, where the remaining $30\,\%$ of PM flux linkage are attributed to the ferrite magnets. This is in accordance with the theorical considerations presented in section I.

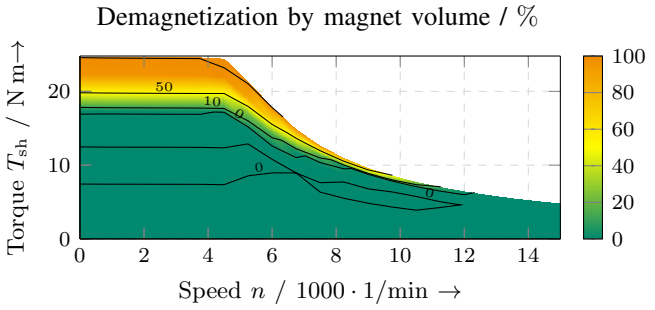

(a) FeN magnets

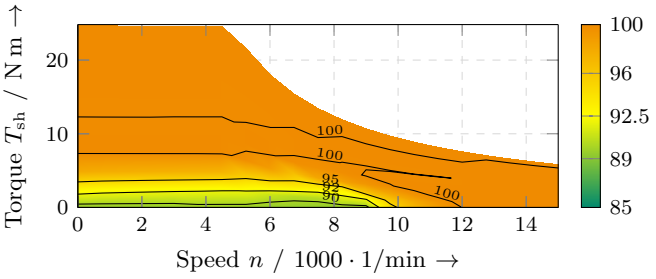

(b) hybrid Magnets

Fig. 8: Demagnetization behavior of magnet 2 in the selected delta machines with $T_{\mathrm{max}} \approx 25\,\mathrm{N\,m}$.

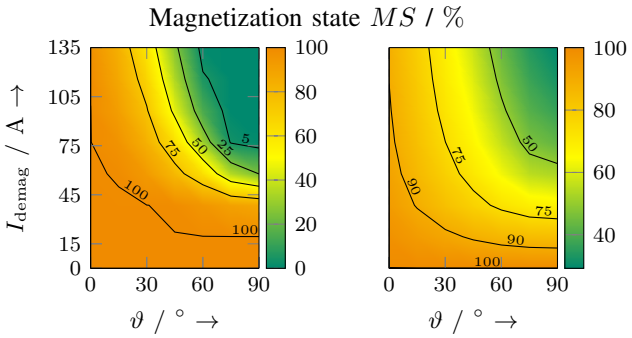

(a) FeN magnets (b) Hybrid magnets

Fig. 9: Demagnetization maps for the selected delta machines with $T_{\mathrm{max}} \approx 25\,\mathrm{N\,m}$.

Both machines' performance is compared in Fig. 10 in the shape of efficiency maps in the torque-speed plane, with the mechanical torque T_{sh} and the rotating speed n. The torque-speed envelope of the other machine is represented as a line in each diagram (i.e. the hybrid machine's M-n-curve in the FeN machines efficiency map and vice versa), to allow a direct comparison of both. The efficiency is calculated based on the optimum MS. Both reach a similar maximum efficiency with $\eta_{\mathrm{FeN}} = 96.4\,\%$ for the FeN and $\eta_{\mathrm{hyb}} = 96.5\,\%$ for the hybrid machine. The hybrid machine has a slightly higher maximum efficiency and a larger operating range with the efficiency beyond $93\,\%$. In the base speed range the behaviour of both machines is similar. The hybrid machine achieves a larger

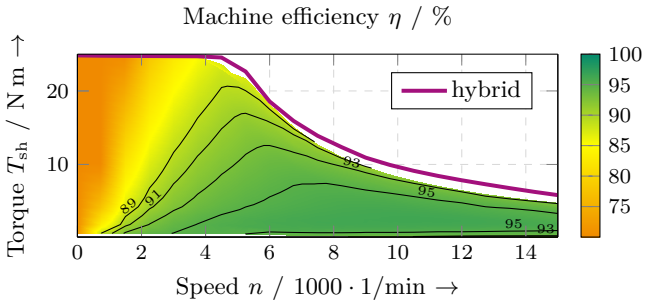

(a) FeN magnets

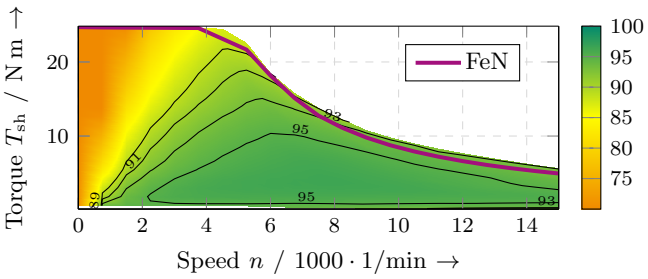

(b) hybrid Magnets

Fig. 10: Efficiency maps of the selected delta machines with $T_{\mathrm{max}} \approx 25\,\mathrm{N\,m}$ under consideration of optimum magnetization state MS.

maximum torque at maximum speed.

V. Conclusion and Outlook

Rare earth free series hybrid variable flux machines with FeN-ferrite magnet combinations were investigated. The behavior of the LCF magnet in the series configuration was analyzed and a method to calculate the magnets' demagnetization throughout a machine's operating range was presented. The ability to demagnetize a hybrid machine was compared to a regular VFM and the findings presented in literature regarding HVFM with NdFeB magnets were confirmed for the rare earth free machines.

The FeN magnets remain an experimental technology with a promising outlook. In electric machines they present an improved performance compared to AlNiCo magnets, albeit they appear to not be commercially available at this point. However, their coercivity is not large enough to function together with ferrite magnets in (serial) HVFM, since the FeN magnets are demagnetized by the ferrite magnet behaving like an additional air gap in the magnetic circuit. The analysis of invidual magnets' demagnetization behavior during operation allows extended analysis and optimization of (H)VFM beyond analytical concepts like magnetic equivalent circuits. Using the methods presented in this work, sensitivity analyses can be carried out.

Measurements on machine prototypes need to be carried out to validate the assumptions presented here. Especially the no-load operating point of the magnets needs critical investigation: For the FEA analyses, idealized geometrical features are assumed to facilitate quick simulations. However, tolerances in manufacturing lead to additional airgaps in the magnet slots, that are difficult to predict in simulations but can lead to demagnetization of LCF magnets under no-load conditions. Further, the demagnetizating and re-magnetizing behavior in a prototype may differ from simulated results: The electrical sheet's simulated properties represent the values measured for the unprocessed sheet material. Typically, the cutting leads to a decrease in performance, thus reducing the flux linkage per current in the machine.

To take advantage of the FeN alloy's properties, investigations into HVFM with AlNiCo magnets as LCF and FeN magnets as HCF will be carried out. This combination appears promising due to the similar remnant flux densities of FeN and AlNiCo. FeN as the HCF magnet has a larger B_{rem} than AlNiCo, which has been proven to be beneficial in series HVFM.

References

[1] European Commission. Directorate General for Internal Market, Industry, Entrepreneurship and SMEs., *Study on the critical raw materials for the EU 2023: final report.* LU: Publications Office, 2023.

[2] V. Ostovic, "Memory motors," *IEEE Industry Applications Magazine*, vol. 9, no. 1, pp. 52–61, Jan. 2003.

[3] K. Sakai, K. Yuki, Y. Hashiba, N. Takahashi, and K. Yasui, "Principle of the variable-magnetic-force memory motor," in *2009 International Conference on Electrical Machines and Systems*. IEEE, 2009, pp. 1–6.

[4] H. Yang, S. Lyu, H. Lin, Z.-q. Zhu, H. Zheng, and T. Wang, "A Novel Hybrid-Magnetic-Circuit Variable Flux Memory Machine," *IEEE Transactions on Industrial Electronics*, vol. 67, no. 7, pp. 5258–5268, Jul. 2020.

[5] M. Ibrahim and P. Pillay, "Design of Hybrid Variable Flux Motors for Enhanced Wide-Speed Performance," in *2019 IEEE Energy Conversion Congress and Exposition (ECCE)*. IEEE, Sep. 2019, pp. 6046–6053.

[6] H. Hua, Z. Q. Zhu, A. Pride, R. P. Deodhar, and T. Sasaki, "A Novel Variable Flux Memory Machine With Series Hybrid Magnets," *IEEE Transactions on Industry Applications*, vol. 53, no. 5, pp. 4396–4405, Sep. 2017.

[7] A. Athavale, K. Sasaki, B. S. Gagas, T. Kato, and R. D. Lorenz, "Variable Flux Permanent Magnet Synchronous Machine (VF-PMSM) Design Methodologies to Meet Electric Vehicle Traction Requirements with Reduced Losses," *IEEE Transactions on Industry Applications*, vol. 53, no. 5, pp. 4318–4326, Jan. 2017.

[8] X. Zhao, H. Lin, Y. Zhong, W. Liu, and H. Yang, "A Novel Separated Hybrid-Magnetic-Circuit Variable Flux Memory Machine," *IEEE Transactions on Industrial Electronics*, vol. 70, no. 12, pp. 12 060–12 070, Dec. 2023.

[9] W. Liu, H. Yang, H. Lin, S. Lyu, and Y. Zhong, "A Novel Variable Flux Memory Machine With Separated Series–Parallel PM Structure," *IEEE Transactions on Industrial Electronics*, vol. 70, no. 4, pp. 3348–3361, Apr. 2023, publisher: Institute of Electrical and Electronics Engineers (IEEE).

[10] M. S. Mirazimi, C. Chen, P. Pescetto, S. Ferrari, G. Pellegrino, M. Diana, and T. Thiringer, "Accurate Modeling of Variable- Flux PMSMs without Electromagnetic Co-Simulation," in *2024 International Symposium on Power Electronics, Electrical Drives, Automation and Motion (SPEEDAM)*. Napoli, Italy: IEEE, Jun. 2024, pp. 625–630.

[11] R. Wilson, P. Kumar, and A. El-Refaie, "Comparative Analysis and Optimization of Iron Nitride Enabled 800-V PM-Assisted Synchronous Reluctance Traction Motor with Varying Poles for Extended Operating Speed Range," in *2024 International Conference on Electrical Machines (ICEM)*. Torino, Italy: IEEE, Sep. 2024, pp. 1–7.

[12] R. Wilson, P. Kumar, A. Al-Qarni, Q. Ma, and A. El-Refaie, "Robustness of Dynamic FEA-based Demagnetization Calculation in the Multi-Objective Optimization of PM-assisted Synchronous Reluctance Motor with Blended Magnets," in *2023 IEEE International Electric Machines & Drives Conference (IEMDC)*. San Francisco, CA, USA: IEEE, May 2023, pp. 1–7.

[13] A. Al-Qarni and A. EL-Refaie, "Design and Optimization of High-Performance Rare-Earth Free Interior Permanent Magnet Motors for Electric Vehicles Enabled by Iron Nitride Magnets," in *2023 IEEE Energy Conversion Congress and Exposition (ECCE)*. Nashville, TN, USA: IEEE, Oct. 2023, pp. 4082–4089.

[14] I. Dirba, M. Mohammadi, F. Rhein, Q. Gong, M. Yi, B.-X. Xu, M. Krispin, and O. Gutfleisch, "Synthesis and magnetic properties of bulk α''-Fe16N2/SrAl2Fe10O19 composite magnets," *Journal of Magnetism and Magnetic Materials*, vol. 518, p. 167414, Jan. 2021.

[15] J. Kesten, F. Frölich, F. Wittemann, J. Knirsch, F. Bechler, L. Kärger, P. Eberhard, F. Henning, and M. Doppelbauer, "Design Approach for a Novel Multi Material Variable Flux Synchronous Reluctance Machine without Rare Earth Magnets," in *2022 International Conference on Electrical Machines (ICEM)*. IEEE, 2022, pp. 2304–2310.

[16] A. M. Technologies, "Cast ALNICO Permanent Magnets," Feb. 2003. [Online]. Available: https://www.arnoldmagnetics.com/wp-content/uploads/2017/10/Cast-Alnico-Permanent-Magnet-Brochure-101117.pdf

[17] H. Yang, Y. Jie, X. Guo, J. Li, and M. Wang, "Investigation of magnetization characteristics of variable flux PM based on a Fourier-fitting hysteresis model," *AIP Advances*, vol. 9, no. 9, p. 095056, Jan. 2019.

[18] H. M. Ltd., "Permanent Magnets," 2016. [Online]. Available: https://hitachi.co.in/pdf/resources/high-function-materials-and-components/advanced-materials-and-components/hg-a27-f.pdf

[19] M. Greule, M. Boxriker, B. Zhang, and M. Doppelbauer, "Numerical iron loss computation method for switched reluctance motors," in *2016 18th European Conference on Power Electronics and Applications (EPE'16 ECCE Europe)*. Karlsruhe: IEEE, Sep. 2016, pp. 1–10.